buildings

MDPI

Article

Experimental Simulation of Deformation Effect Propagation Due to Explosion on the Surface of a Small-Scale Model

Daniel Papán [1,*], Emma Brozová [2] and Zuzana Papánová [1]

[1] Department of Structural Mechanics and Applied Mathematics, Faculty of Civil Engineering, University of Žilina, Univerzitná 8215/1, 010 26 Žilina, Slovakia
[2] Faculty of Civil Engineering, University of Žilina, Univerzitná 8215/1, 010 26 Žilina, Slovakia
* Correspondence: daniel.papan@uniza.sk; Tel.: +421-948-037947

Abstract: The use of small-scale models is an important area of research today. An investigation is conducted on the response of a small-scale model's vibrating surface. For this model, a small-scale surface explosion is used for loading. According to the article, the methodology includes procedures, model development, the explosive materials used, measurement and evaluation methods, software, and the technique used. Signal processing and response evaluation rely on a scientific method—the backward Fourier-transform principle—for frequency filtering. In this study, the simulation results are used to confirm the basic physical properties of the viscoelastic system. It is primarily investigated whether wave processes are confirmed on the new material. In terms of single wave propagation, the results summarize the characteristics of these waves (attenuation, velocity of propagation, etc.). Conclusions are targeted at the possibility of correlating three types of results: small-scale simulations, numerical simulations, and a real full-scale experiment.

Keywords: acceleration; small-scale; explosion; measurement

check for updates

Citation: Papán, D.; Brozová, E.; Papánová, Z. Experimental Simulation of Deformation Effect Propagation Due to Explosion on the Surface of a Small-Scale Model. *Buildings* **2023**, *13*, 1566. https://doi.org/10.3390/buildings13061566

Academic Editor: Enrico Tubaldi

Received: 13 October 2022
Revised: 7 June 2023
Accepted: 16 June 2023
Published: 20 June 2023

1. Introduction

Every building's structure is affected by a certain type of load. In general, these can be categorized according to three main sources. The majority of the load is generated by gravity. It is the structure's own deadload that has to be dealt with in this case.

Another large group is the imposed or live loads resulting from the use of the structure. Climatic conditions also have a major influence. The last group of loads comprises the special loads that will be dealt with in this work. Special loads typically occur irregularly and are of significant magnitude and short duration. Dynamic loads are defined by the character of their response [1,2].

In contrast to static loads, dynamic loads are variable in time, and the effects of inertial forces must also be taken into consideration. When it comes to building structures, load frequencies between 0.1 and 500 Hz play a crucial role. The major damage occurs mainly in the frequency range from 1 to 150 Hz. The impact caused by explosions has a frequency range from 1 to 40 Hz; therefore, attention must be given to this aspect.

One of the reasons why we have to deal with explosions is that we are unable to fully understand how they affect objects at small distances. As long as we are capable of clarifying the process, we may be in a position to save the lives of people around the world. This is because we will be able to predict the behavior of this type of load and then take the necessary precautions. A variety of fields are becoming increasingly concerned with the effects of explosions on building structures.

The propagation of blast effects is a complex phenomenon, which is not yet well understood. This paper presents an experimental simulation of effects of deformation propagation due to explosions on the surface of a small-scale model [3,4].

The number of victims of terrorist attacks and explosions caused by explosives continues to increase, and we arere looking for ways to prevent these and minimize their consequences. The goal is to learn more about how blast waves move in order to better protect people and buildings from this type of attack. The purpose of this paper is to give a basic understanding of blast loading. Critical infrastructures, such as public transport or other places where large numbers of people are likely to congregate, are especially at risk from terrorist attacks. This is a serious issue for many countries, and is something that needs to be taken into account in the design of buildings and of infrastructure in general.

Many researchers have studied the dynamics of shock waves after the topic was first investigated in the early 1950s. The first analytical solution to the problem of wave propagation from explosions was given by G. I. Taylor [5]. Much study in this field followed. With the aid of high explosives, Jack et al. [6] simulated the effects of a blast at altitude.

2. Materials and Methods

An explosion occurs when a large amount of energy is suddenly released and turned into power. The explosion causes a rapid increase in pressure, which is usually followed by sound, light, and heat effects.

The blast can reach a velocity of more than 1000 $m \cdot s^{-1}$, and the result is usually the damage to or complete destruction of nearby structures and facilities. According to the type and source of the reaction, explosions can be classified as atomic, mechanical (physical), and chemical. Building structures are most often threatened by explosions of a chemical nature. The parameters of the pressure wave are also significantly affected by the environment, whether the explosion occurs in an open or a confined space [7].

A chemical explosion is a rapid reaction or change in state. Exothermic breakdown of a chemical produces heat, gas, and vapor. Because the reaction occurs promptly and the reacted components do not expand instantly, the explosion products take up the space previously occupied by the explosive as shown in Figure 1 [8].

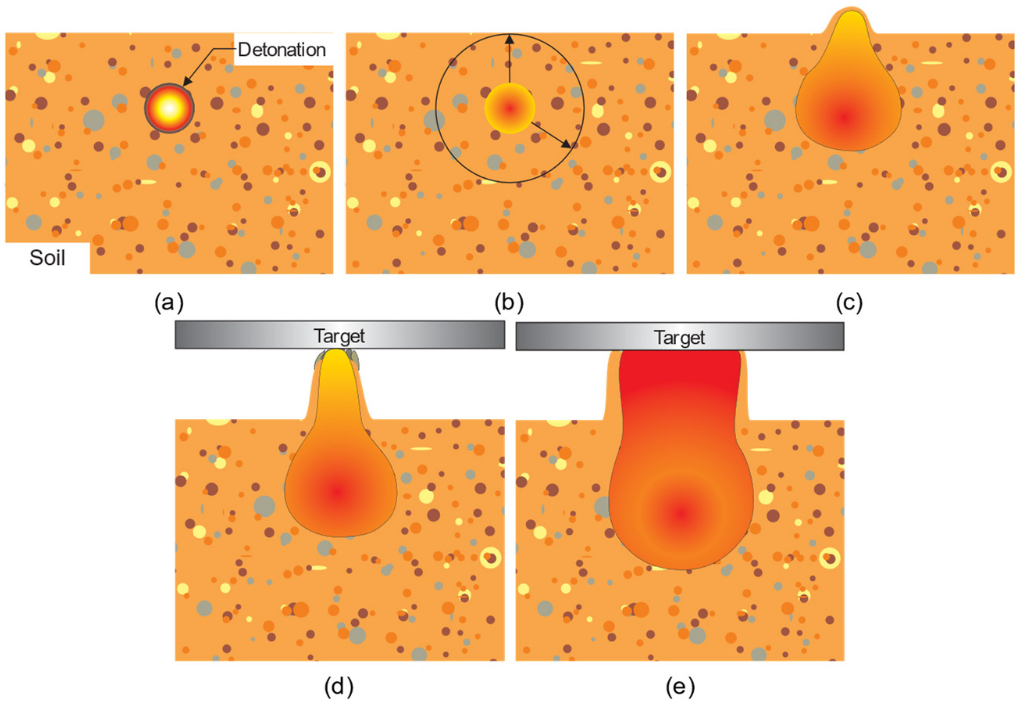

Figure 1. Five stages of a shallow buried detonation. (**a**) Detonation of the chemical explosive; (**b**) interaction between detonation shock wave and expanding detonation products into the surrounding soil; (**c**) expansion of the soil and detonation products into free air; (**d**) early interaction with the target; (**e**) late interaction with the target [8].

The high rate of chemical transformation, the exothermic aspect of the chemical reaction, the spontaneous propagation of the reaction, and the ability to transform thermal energy into mechanical energy all contribute to a chemical explosion. Substances capable of chemical transformation are called explosives [9].

2.1. Determination of Explosion Energy

The Trinity test in New Mexico in 1945 resulted in the explosion of the first atomic bomb as shown in Figure 2. A few years later, a popular magazine released a number of images of the explosion along with a timeline and range scale. British scientist G. I. Taylor calculated the explosion's energy output from these photos. The idea behind it is to utilize dimensional analysis to predict how the radius will change in relation to other physical parameters [10]. The following equation, which describes the radius as a function of time, energy, and density, is used to quantify the amount of energy in an explosion.

$$r = f(t; E; \rho) \tag{1}$$

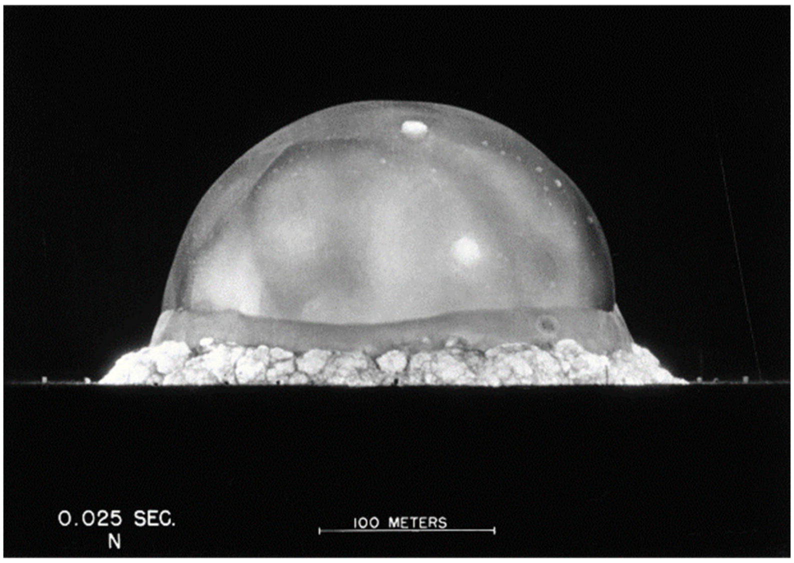

Figure 2. Screenshot showing the exact time and size scale of the explosion of the first atomic bomb taken from a video [11].

After substituting the variables and modifying the equation:

$$[m] = [s][\text{kg}\cdot\text{m}^2\cdot\text{s}^{-2}][\text{kg}\cdot\text{m}^{-3}] \tag{2}$$

$$[r] = [t^a \cdot E^b \cdot \rho^c] \tag{3}$$

$$m = s^a \cdot (\text{kg}\cdot\text{m}^2\cdot\text{s}^{-2})^b \cdot (\text{kg}\cdot\text{m}^{-3})^c \tag{4}$$

The linear equations are solved, and the exact values are determined:

$$a = \frac{2}{5}; b = \frac{1}{5}; c = -\frac{1}{5} \tag{5}$$

These are substituted into Equation (4):

$$[r] = \left[t^{\frac{2}{5}} \cdot E^{\frac{1}{5}} \cdot \rho^{-\frac{1}{5}}\right] \tag{6}$$

After the following modification:

$$[r] = \left[\left(\frac{t^2 \cdot E}{\rho}\right)^{\frac{1}{5}}\right] \tag{7}$$

The resulting equation has the formula:

$$r = C \cdot \left(\frac{t^2 \cdot E}{\rho} \right)^{\frac{1}{5}} \tag{8}$$

where:

C—based on small-scale measurements, C = 1033 represents the ratio between time and radius;
ρ—ambient air density;
r; t—measured data.

2.2. Seismic Wave Types

As previously mentioned, explosions release a considerable amount of energy. From the source, this spreads in several ways (Figures 3 and 4). There are four fundamental types of waveform:

1. Longitudinal P-waves—primary. These are the fastest type of waves and reach the accelerometers first. Both P-waves and pressure waves move in the same direction. The material that is affected by a pressure wave moves forward and then back along the same path as the wave when it reaches a certain point.
2. Transverse S-waves—secondary. In the case of accelerometers, they arrive as secondary signals. When the wave passes through the material, the point of propagation moves from side to side or up and down.
3. Love waves—surface waves. Like S-waves they oscillate the surface from side to side in the direction they propagate.
4. Rayleigh waves—the second type of surface waves. As a result, the surface moves simultaneously in both vertical and horizontal directions. Due to their potential for causing significant damage to buildings and other structures, these waves are extremely dangerous [12].

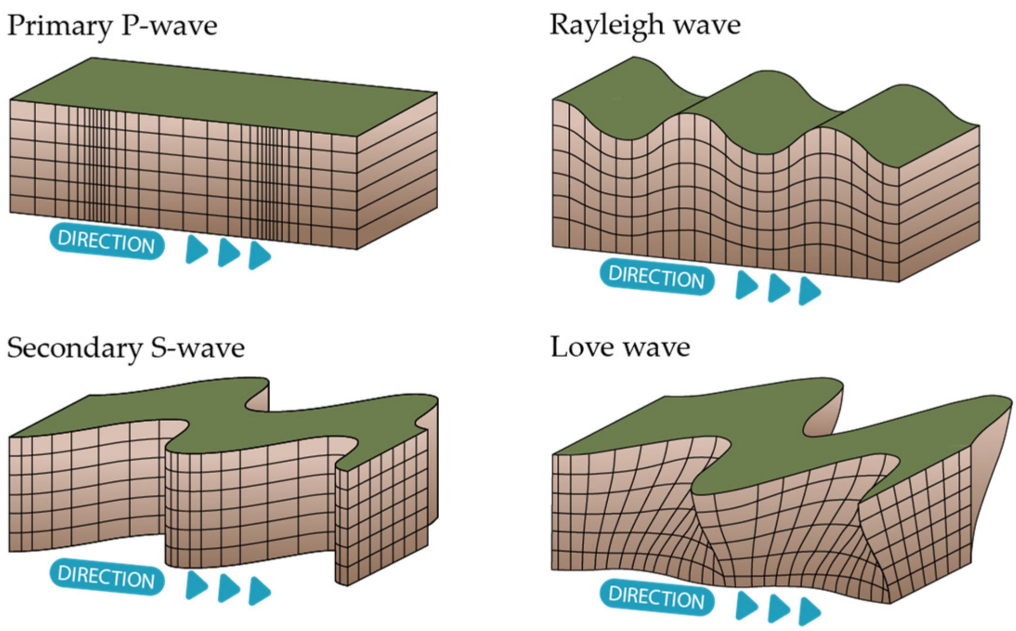

Figure 3. Seismic wave types and their propagation shape in the subsurface.

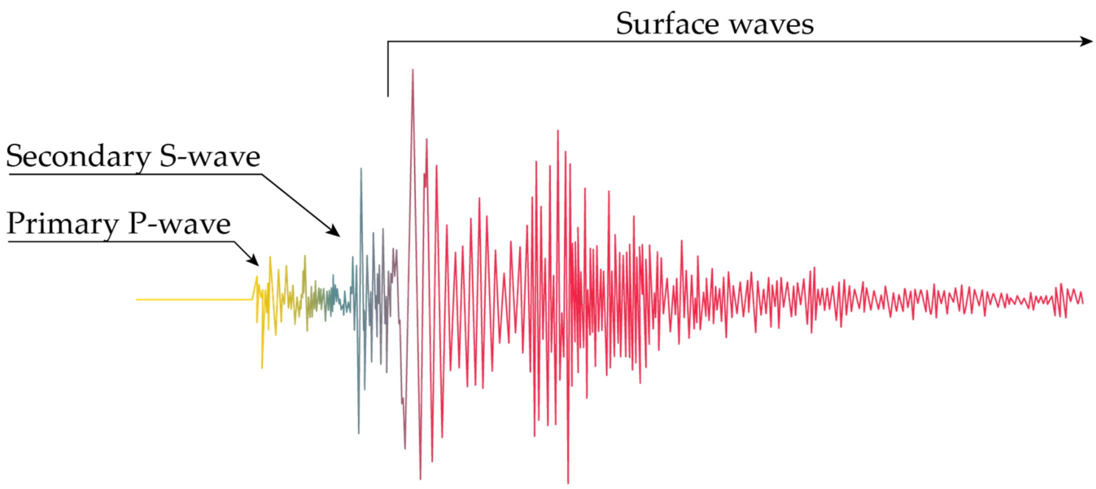

Figure 4. A simplified seismic recording that captures the primary P-wave, secondary S-wave, and surface waves.

2.3. Explosives

Explosives are chemical compounds which, if properly activated, are capable of rapid chemical or physical-chemical action, and can release large amounts of energy with the associated release of large amounts of gases and accompanying light, heat, and sound effects [9].

Black powder is the world's earliest known explosive, having been developed in China. It is made up of potassium nitrate (75%) (Figure 5), charcoal (15%), and sulfur (10%). It is currently used as a timing powder, to make delay compositions, as well as powder bodies for initiators, fuses, and pyrotechnic compositions. The properties of black powder are variable according to its composition, grain shape and size, and the charcoal used [13].

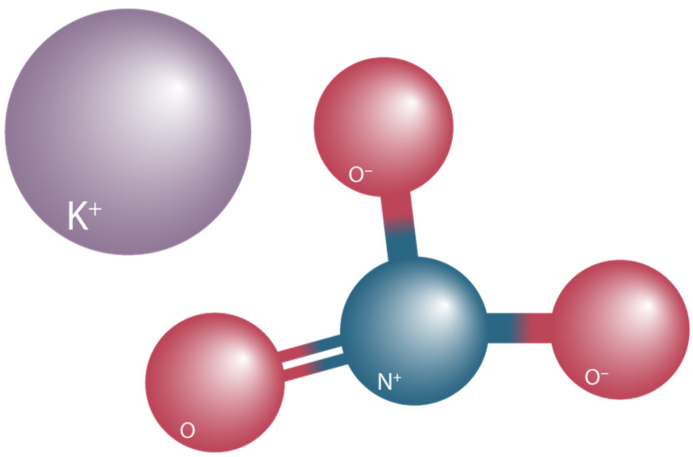

Figure 5. Molecular structure model of potassium nitrate KNO_3.

Explosives are classified into four categories: munitions, crackers, blasting agents, and pyrotechnic compositions.

2.3.1. Pyrotechnic Compositions

It is a mechanical mixture of combustibles and oxidizing substances, perhaps with additional additives to achieve the desired technical effect. Exothermic reactions are used to produce heat, light, gas, smoke, and sound. Pyrotechnic compounds are classified based on these properties into the following categories: light, flash, smoke, incendiary, and special. A wide variety of oxidizing substances are used in pyrotechnic compositions, including oxides and peroxides, nitrates, chlorates, and some crystalline salts. Furthermore, binders, flame coloring additives, fume colorants, special effect enhancers, phlegmatizers, stabilizers, flame accelerators or retardants, and solvents may be used [9]. There is also the possibility of rapid combustion escalating into an explosive phase. For a number of purposes, including fireworks, firecrackers, smoke bombs, timers, sound effects, etc., they are used by civilians, police, and also military forces.

2.3.2. Fireworks

The term 'fireworks' refers to all pyrotechnic items which contain various chemical compounds and mixtures which, when ignited, produce sound or light effects. The majority of sound effects produced by fireworks are composed of firecrackers, while the majority of light effects are derived from sparklers, flares, light cascades, etc. As a result of their use, purpose, and degree of danger, as well as the level of noise, fireworks can be divided into four categories:

1. Category F1—this category is considered to be very low risk and noise levels are negligible. Only persons over the age of 15 are permitted to purchase this product. This includes, e.g., sparklers, fountains, and buzzers.
2. Category F2—represents a low level of danger and minimal noise levels. A person must be at least 18 years of age in order to purchase this product. Among these items are, for example, cannons, rockets, compacts, and fountains.
3. Category F3—presents a medium level of danger and the noise level is not harmful to human health. The product is only available to persons over the age of 21. A few examples of this type of fireworks would be firecrackers, compacts and rockets.
4. Category F4—a major level of danger is associated with this category, which includes professional pyrotechnics that are available only to qualified users [14].

2.3.3. K01M Booming Carpet

Experimental measurements were conducted using K01M Blasting Carpet firecrackers manufactured by Klásek Trading, s.r.o. The package contains five carpets with 70 small firecrackers each. The firecracker is classified as F2 and the mass of the pyrotechnic composition is 3.5 g per carpet, which is 0.05 g per single firecracker. The product is primarily composed of a flash component based on the principle of potassium chlorate and aluminum powder, probably in a ratio of 7:3.

Equation (9) represents an oxidation–reduction reaction in which potassium chlorate $KClO_4$ is the oxidizing agent and aluminum Al is the reducing agent. At the same time, these two chemicals are reactants, and the resulting products are aluminum oxide Al_2O_3 and potassium chloride KCl. In order for the reaction to occur, a temperature between 600 and 700 degrees Celsius must be reached.

$$3KClO_4 + 8Al \rightarrow 4Al_2O_3 + 3KCl \tag{9}$$

Potassium chlorate $KClO_4$ is used as an oxidizing agent. It is a colorless crystalline substance that has a wide range of applications in pyrotechnics. In order to achieve the desired lighting effects, it is most commonly mixed with sulfur, aluminum, or magnesium.

There are numerous applications for aluminum powder in various fields. In most cases, it is used as a gas-forming additive in aerated concrete, rocket fuel, cosmetic dyes, and pyrotechnics, where it contributes to the balance of oxygen levels and accelerates combustion in combination with potassium perchlorate [13].

2.4. Experimental Measurement

An essential role is played by experimental analyses in verifying the results of various studies. These measurements were conducted in order to demonstrate that all types of waves are initiated in a small-scale explosion, and based on the measured data, we can determine the shear wave velocity and demonstrate the presence of dispersive attenuation.

2.4.1. Description of Measurement Equipment

An appropriate measuring apparatus was necessary in order to make the actual measurements. Among these items are accelerometers, module, laptop, and accessories. Additionally, a vibration calibrator was used.

Accelerometers—DeltaTron Brüel & Kjær type 4508 B 002 (Figure 6). Its high sensitivity, light weight, and small size make this type of accelerometer ideal for modal measurements. The frequency range is between 0.4 Hz and 8000 Hz and the coaxial connector is perpendicular to the main axis that needs to be detected [15].

Figure 6. DeltaTron accelerometer Brüel & Kjær type 4508 B 002.

Module—PULSE LAN-XI Brüel & Kjær type 3050-B-060 (Figure 7). In this module, there are six channels that are designed to provide the widest possible coverage of applications relating to sound and vibration measurement. In terms of frequency range, it operates between 0 kHz and 51.2 kHz [16].

Figure 7. Module PULSE LAN-XI Brüel & Kjær type 3050-B-060.

Vibration calibrator—Metra Mess VC21 (Figure 8) is used to calibrate vibration measurement and control systems. It is based on the principle of generating mechanical vibrations at a steady frequency. In total, there are seven frequencies ranging from 15.915 Hz to 1280 Hz [17].

Last but not least, it is important to mention the SigView. This program is a real-time signal analysis software that offers a number of powerful signal analysis tools, as well as statistical functions and a comprehensive visualization platform [18].

Figure 8. Metra Mess Vibration Calibrator VC21.

2.4.2. Small-Scale Model

In general, the model (Figure 9) is made up of two main components, namely the simulation mass and the vertical wall that prevents the reflection of acoustic waves. The material chosen for this project was polystyrene for practical reasons. In relation to the investigational simulation mass, the material of the mold was chosen to be sufficiently rigid, and at the same time, its properties minimized the reflection of waves. In terms of dimensions, the form was created in such a way as to separate the individual types of waves and at the same time preserve the smallest, small-scale nature of the experimental measurement. This created the boundary conditions for this specific type of investigation of wave processes.

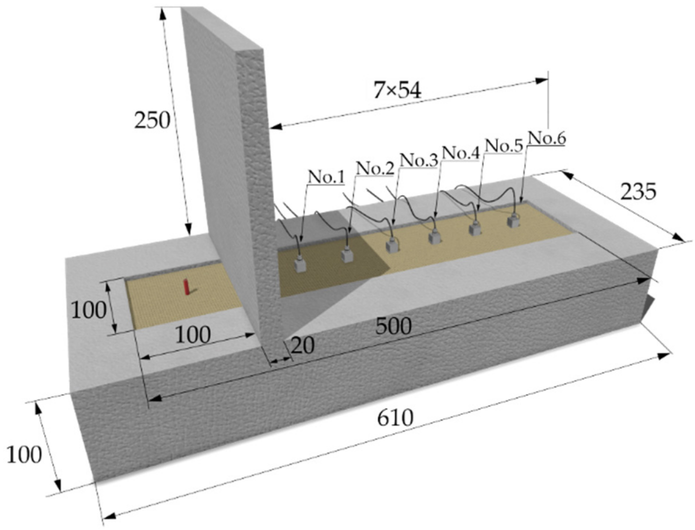

Figure 9. Three-dimensional visualization of the small-scale model that was used for experimental measurements.

Based on a number of literature references, kinetic sand was selected as the simulation material. Kinetic sand is made of 98% sand and 2% polydimethylsiloxane and its properties resemble wet sand. The polydimethylsiloxane (PDMS) gives it a moist appearance and causes it to adhere to itself. As well as being visually clear, PDMS is generally inert, non-toxic, and non-flammable. It is an organic polymer based on silicon and is popular for its liquid properties. In general, the longer the polymer chain, the more flexible it becomes [19].

PDMS is viscoelastic, which means it behaves like a viscous liquid, similar to honey, when flowing for long periods of time (or at high temperatures). However, at short time flows (or low temperatures), it behaves as a rigid elastic solid, comparable to rubber [20]. Overall, PDMS has a low modulus of elasticity, which allows it to deform easily and leads to rubber-like behavior. The viscoelastic characteristics of PDMS may be determined more precisely using dynamic mechanical analysis. The shear modulus varies according to the conditions under which it is prepared, and it then ranges from 100 kPa to 3 MPa [21].

In addition to these mechanical properties, further research will be conducted on cohesion and other properties of the material.

2.4.3. Measurement Methodology

In order to conduct the measurements, six accelerometers were evenly placed within the simulation mass. They were separated by approximately 54 mm along their axis. In the first test, the measurements were performed in the parking lot of the Faculty of Civil Engineering of the University of Žilina. In this instance, a firecracker called DUM BUM F2 was used from Klásek Trading, s.r.o., danger category F2. As a result of this measurement, it was determined that the firecracker was too strong and it was replaced with K01M Booming Carpet firecrackers, which are used in all other measurements. For the purpose of collecting and analyzing sound and vibration data, the PULSE™ Time Data Recorder was used.

Another set of measurements was taken indoors in the laboratory of the Department of Structural Mechanics and Applied Mathematics. Due to the strong reflections within the confined space, the measurement was once again unacceptably inaccurate. A number of other test measurements were conducted without the use of PULSE™. The B&K module type 3050-B-060 is capable of recording data using Internet Explorer. Data are stored directly on the SD card within the module. In this case, the file is saved in the WAV format; however, this format is primarily used for audio recordings. There is no standard for how amplitude values are recorded in terms of units. As a consequence, it was necessary to determine a coefficient for multiplying all the measurement values. This is covered in the next chapter.

The final measurements were conducted outside to prevent the propagation of acoustic waves. Again, a few more measurements had to be taken, which demonstrated that the sensors still needed to be additionally covered. In total, more than 80 measurements were obtained, of which 14 were acceptable and are presented in this paper. In essence, the amplitude of the last accelerometer tended to increase (Figure 10). The reason for this was probably due to the small-scale model, in which the last accelerometer was capturing waves that were already reflected. For operational reasons, it was not possible to take measurements in open space. Due to this, even though the measurements were conducted outside, there were always nearby buildings from which the aforementioned reflected waves occurred. This accelerometer was later removed from the analysis, as will be explained further below. However, establishing this fact required multiple inaccurate measurements. It also happened occasionally that, for unknown reasons, the amplitude started to have a rising tendency on the 4th accelerometer (Figure 11). It can only be assumed that there was a loose connection between the cable and the accelerometer. Afterwards, it became necessary to make a very precise check for every single measurement. When collecting data, it is crucial to choose a reliable measuring method. It took a process of trial and error to figure out how to take measurements correctly (Figures 12–14). Another 20 measurements were carried out for calibration.

2.4.4. Determination of the Scaling Coefficient

It was necessary to calculate the coefficient that multiplied all the values from the individual measurements in order to be able to work with the measured data. Here is how the process worked. The first record was made using a vibration calibrator on which the accelerometer was positioned using calibration support. During a continuous recording of the PULSE™ system, the frequencies on the vibration calibrator were changed. A frequency of 15.92 Hz was the lowest and a frequency of 1280 Hz was the highest. The recording was conducted at accelerations of 1 $m \cdot s^{-2}$ and 2 $m \cdot s^{-2}$. These data were then exported from the PULSE™ system as a CSV file and analyzed in SigView software version 3.0.2.0. Second, a B&K 3050-B-060 module was used, which produced a WAV file as the output. In order to determine the coefficient, the maximum amplitude at each frequency was determined. From this value, a ratio and then an average were calculated. Tables 1–3 present all of the gathered data.

Table 1. The maximum amplitudes obtained in the PULSE™ system.

Frequency	Amplitude $1\ m{\cdot}s^{-2}$	Amplitude $2\ m{\cdot}s^{-2}$
15.92 Hz	1.1813	2.3387
40 Hz	1.4208	2.7480
80 Hz	1.4085	2.7809
0 Hz	1.3988	2.7759
320 Hz	1.3897	2.7599
640 Hz	1.4201	2.7716
1280 Hz	1.4053	2.7592

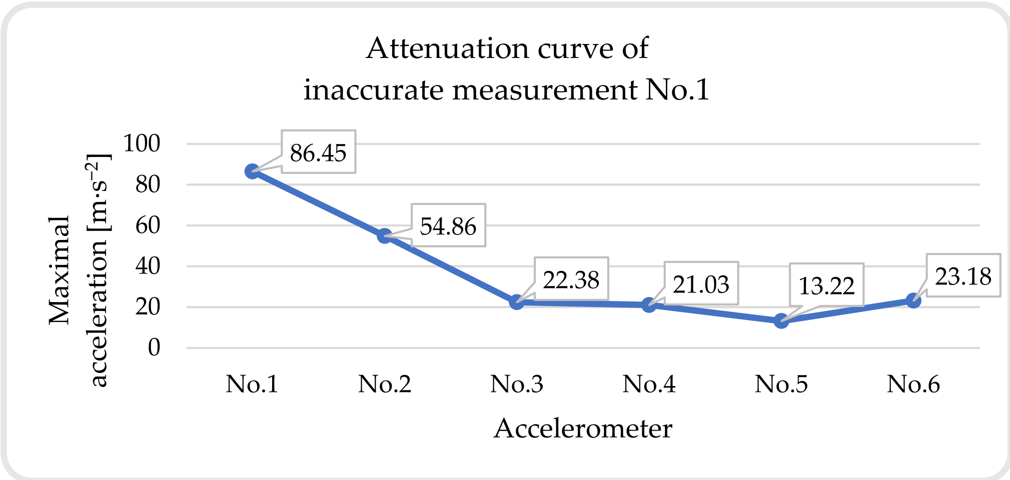

Figure 10. Attenuation curve of inaccurate measurement No.1 with representation of maximum amplitudes at each accelerometer.

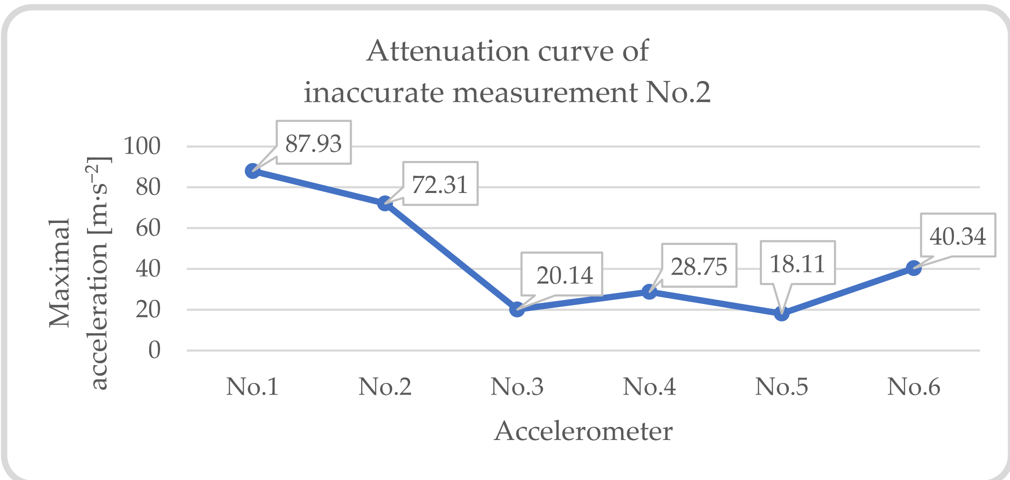

Figure 11. Attenuation curve of inaccurate measurement No.2 with representation of maximum amplitudes at each accelerometer.

Figure 12. Model from the first outdoors test measurement in a parking lot.

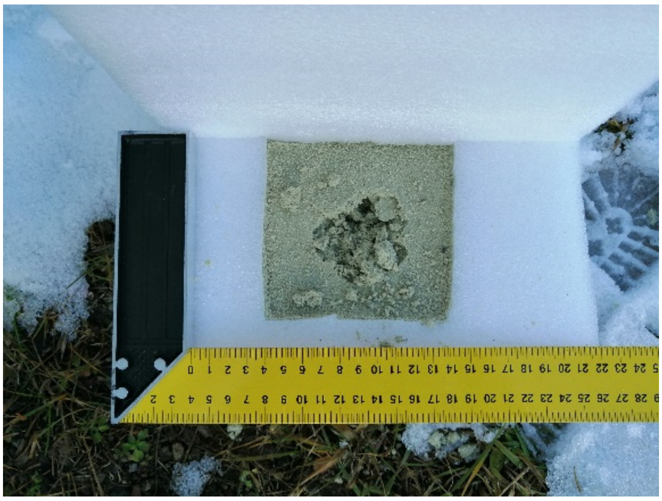

Figure 13. Result of the explosion of the firecracker DUM BUM F2 from the first measurement.

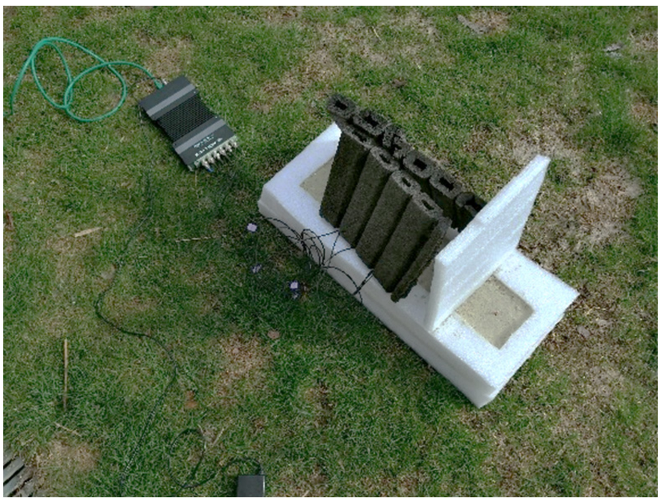

Figure 14. Measurement model with extra covered accelerometers.

Table 2. The maximum amplitudes obtained with the B&K module.

Frequency	Amplitude $1\ m{\cdot}s^{-2}$	Amplitude $2\ m{\cdot}s^{-2}$
15.92 Hz	32.631	62.751
40 Hz	32.736	63.163
80 Hz	31.959	62.595
160 Hz	30.902	62.066
320 Hz	30.832	62.511
640 Hz	31.238	63.855
1280 Hz	31.424	62.525

Table 3. The determination of the final coefficient.

Frequency	Ratio CSV/WAV $1\ m{\cdot}s^{-2}$	Ratio CSV/WAV $2\ m{\cdot}s^{-2}$
15.92 Hz	3.62018×10^{-5}	3.72695×10^{-5}
40 Hz	4.34018×10^{-5}	4.35065×10^{-5}
80 Hz	4.40721×10^{-5}	4.44269×10^{-5}
160 Hz	4.52657×10^{-5}	4.47250×10^{-5}
320 Hz	4.50733×10^{-5}	4.41506×10^{-5}
640 Hz	4.54607×10^{-5}	4.34046×10^{-5}
1280 Hz	4.47206×10^{-5}	4.41295×10^{-5}
Average:	4.34566×10^{-5}	4.30875×10^{-5}
Final coefficient:	4.3272×10^{-5}	

3. Results

The measured data were analyzed in the software SigView, and the graphical outputs of SigView represent the results of the experimental measurements. The total number of measurements has exceeded 80, but only 14 have been deemed satisfactory and remained to be processed, as mentioned previously (Figures 15–20). Since all measurements had similar parameters, only one record was analyzed in detail. As a result of the evaluation of the records, it was identified that the last accelerometer, No. 6, exhibits low reflections due to the small-scale model. Therefore, this accelerometer was excluded from the analysis, and it was not considered further, except for measurement No. 1.

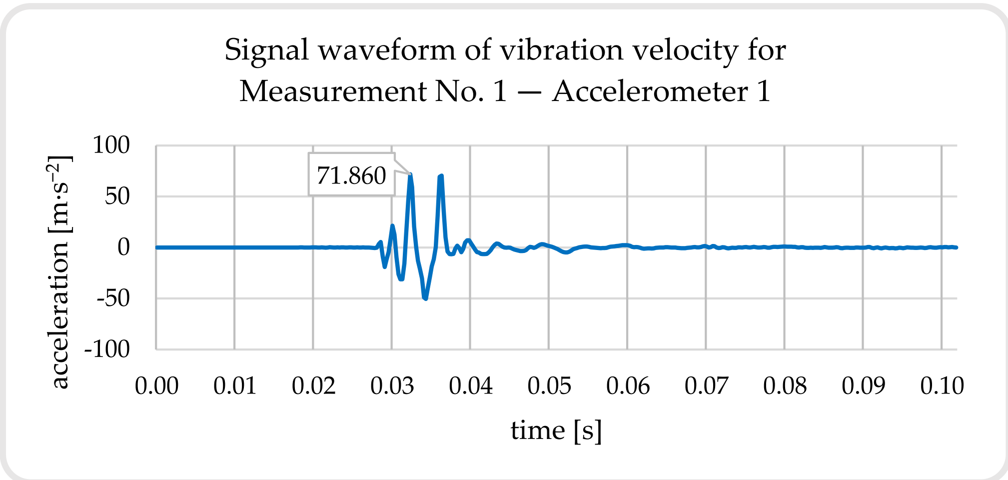

Figure 15. Measurement No. 1—Vibration velocity time history of Accelerometer 1 with maximum amplitude indicated.

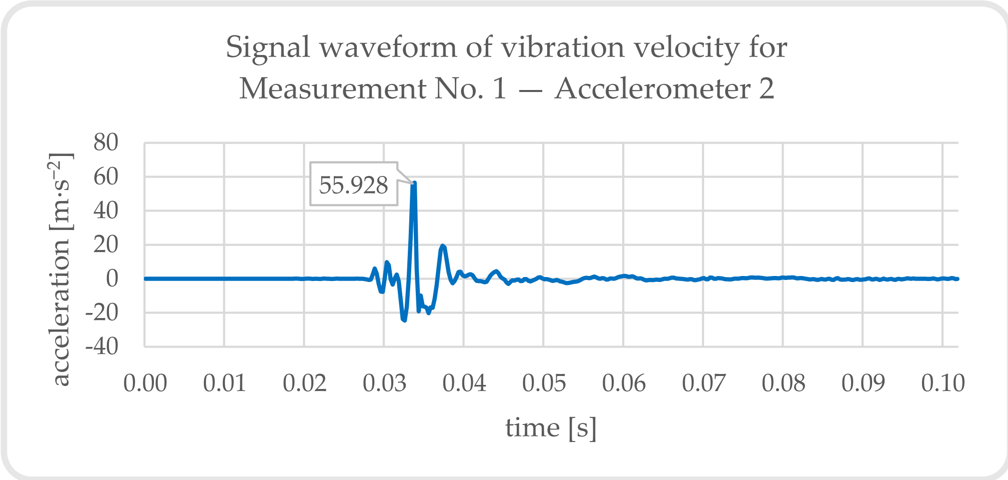

Figure 16. Measurement No. 1—Vibration velocity time history of Accelerometer 2 with maximum amplitude indicated.

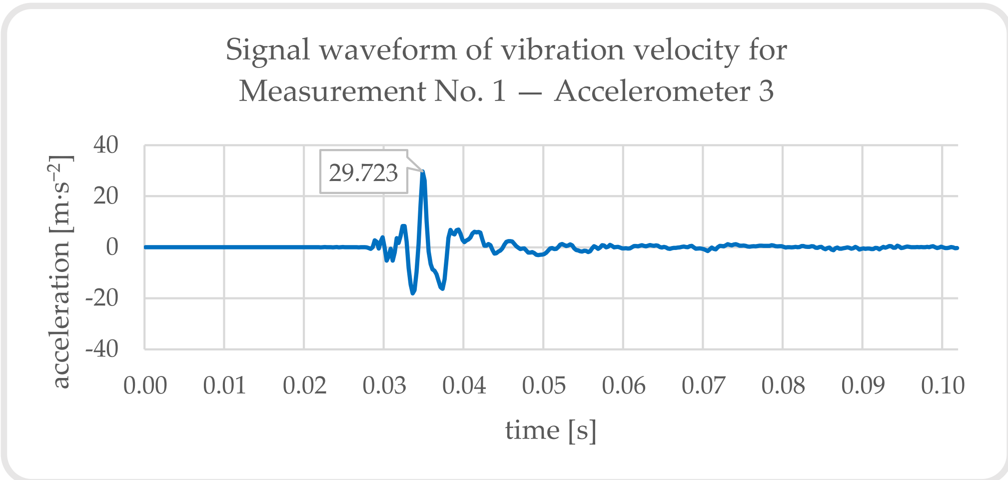

Figure 17. Measurement No. 1—Vibration velocity time history of Accelerometer 3 with maximum amplitude indicated.

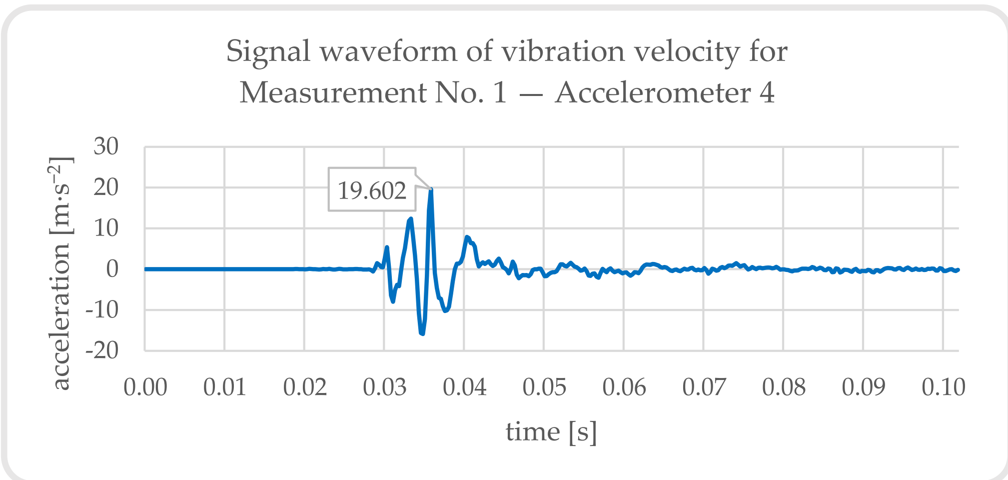

Figure 18. Measurement No. 1—Vibration velocity time history of Accelerometer 4 with maximum amplitude indicated.

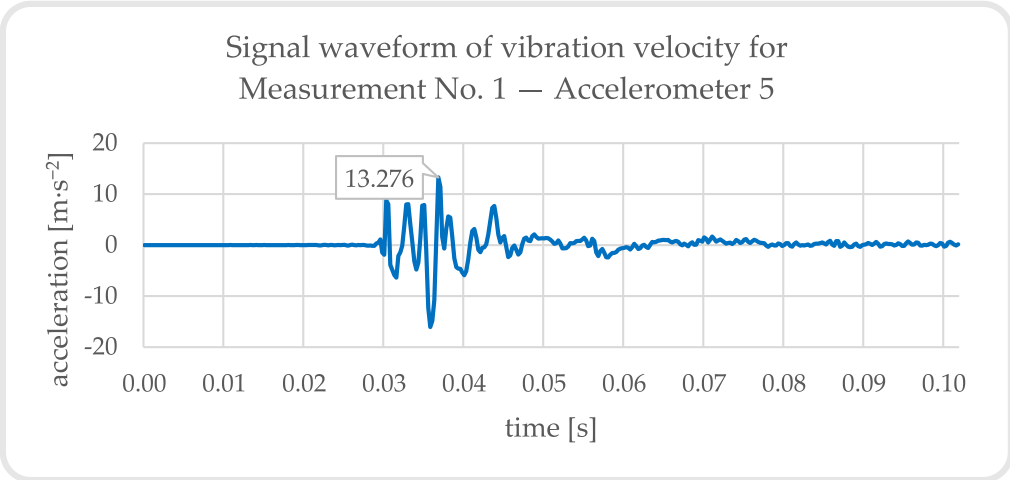

Figure 19. Measurement No. 1—Vibration velocity time history of Accelerometer 5 with maximum amplitude indicated.

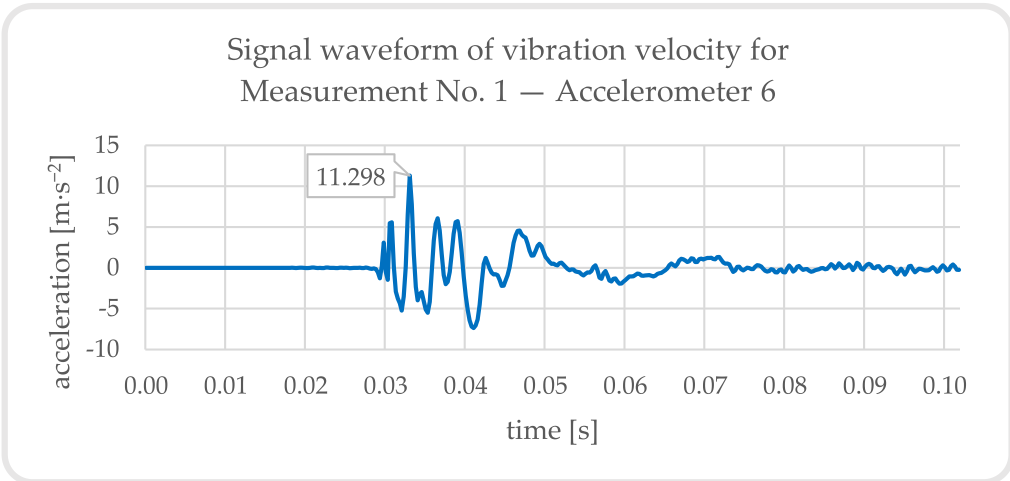

Figure 20. Measurement No. 1—Vibration velocity time history of Accelerometer 6 with maximum amplitude indicated.

To begin with, the WAV file was exported to a CSV file. In MS Excel, each record was opened and the unnecessary data before and after the actual explosion was deleted and multiplied by the calculated coefficient. Only then was it possible to open and analyze the data using SigView. The process was repeated for each measurement and for each accelerometer separately, i.e., 70 times in total. A sampling frequency of 4096 Hz was automatically selected by the module and did not need to be set manually.

Figures 21 and 22 illustrates the waveforms of all types of waves that are generated in an explosion. In order of arrival at the accelerometers, the longitudinal P-wave arrives first, followed by the transverse S-wave, and the surface waves reach the accelerometers last, resulting in the most destructive effects (Figures 23–28 and Table 4). The results are also presented in Figure 29.

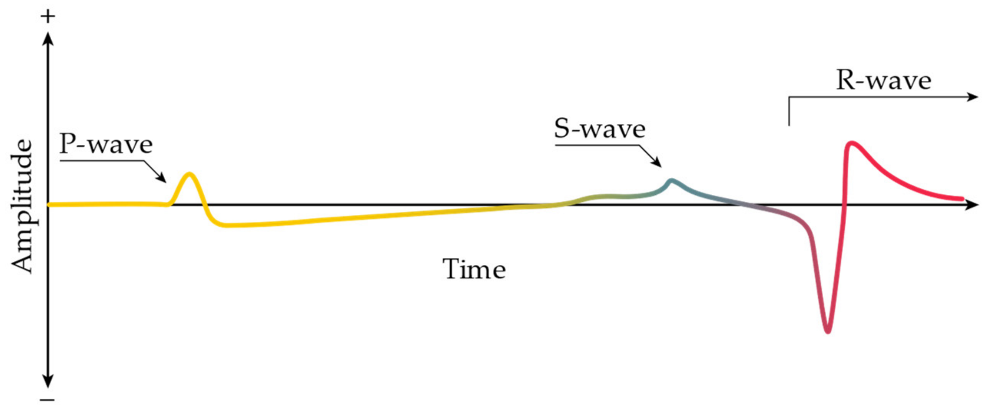

Figure 21. Scheme of the progress of waveform all types of waves during an explosion.

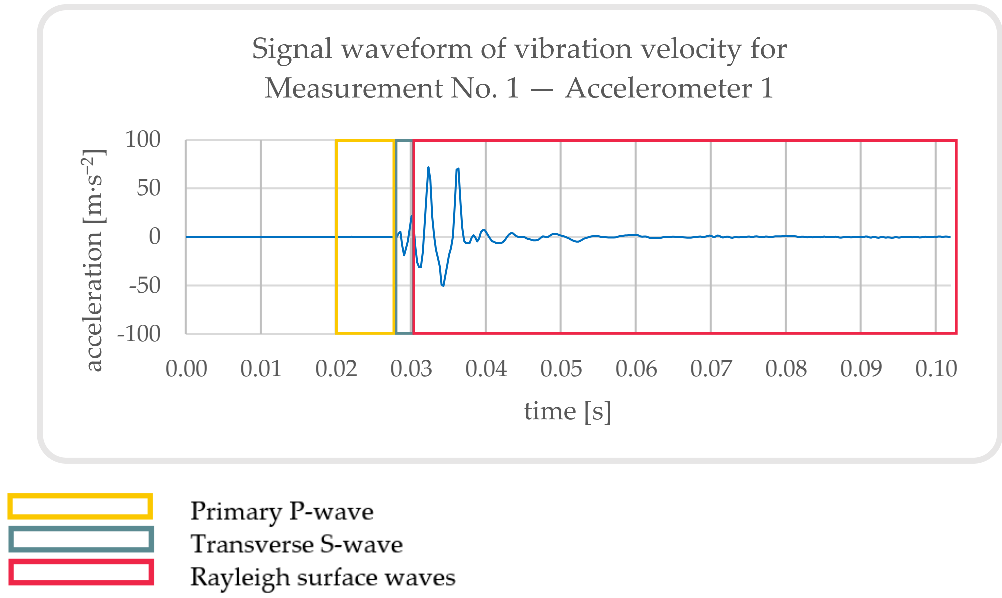

Figure 22. Measurement No. 1—Vibration velocity time history of Accelerometer 1 with graphical representation of the wave types.

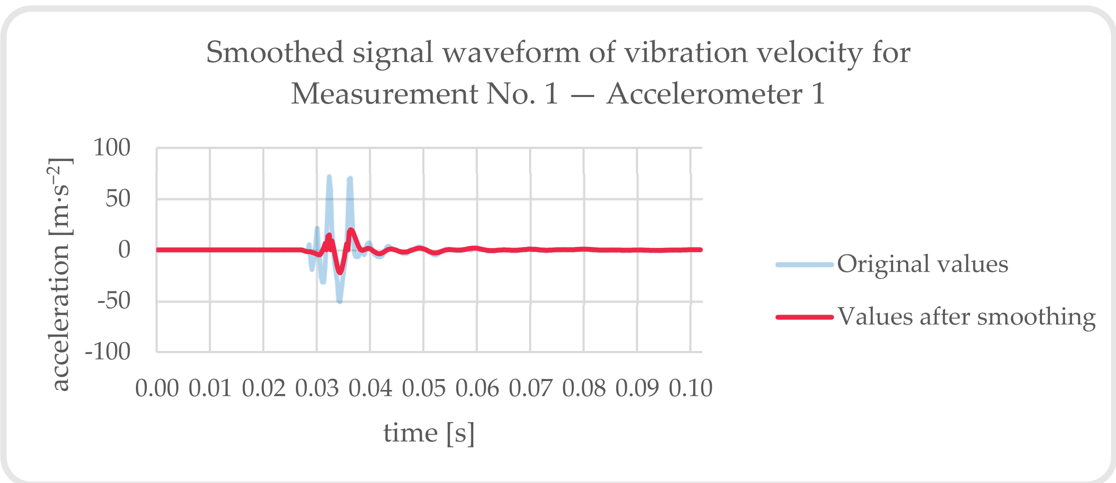

Figure 23. Measurement No. 1—Smoothed vibration velocity time history of Accelerometer 1.

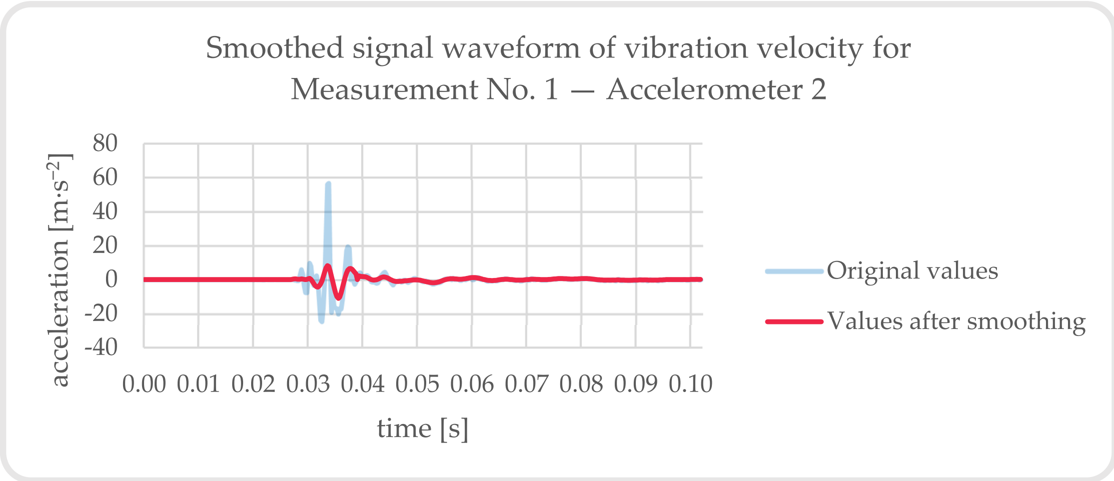

Figure 24. Measurement No. 1—Smoothed vibration velocity time history of Accelerometer 2.

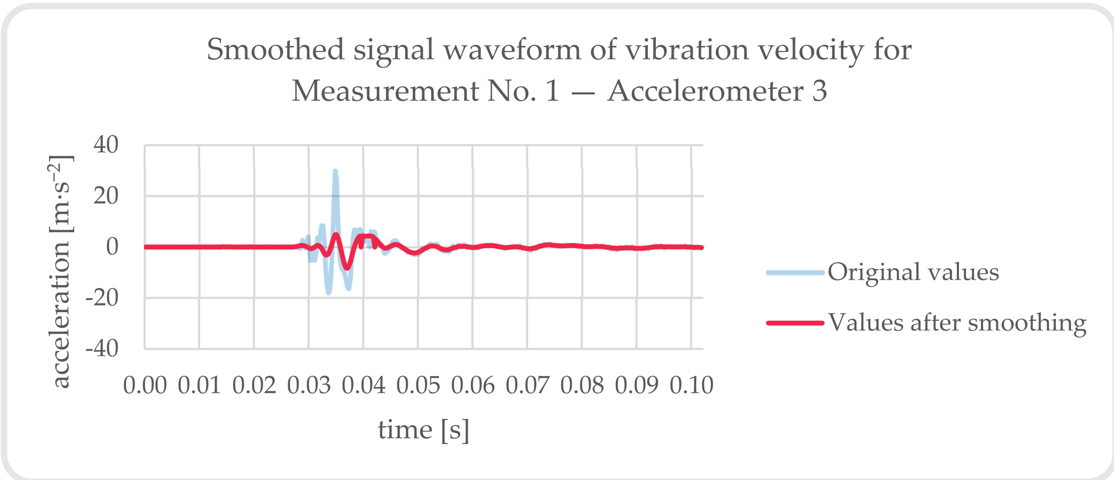

Figure 25. Measurement No. 1—Smoothed vibration velocity time history of Accelerometer 3.

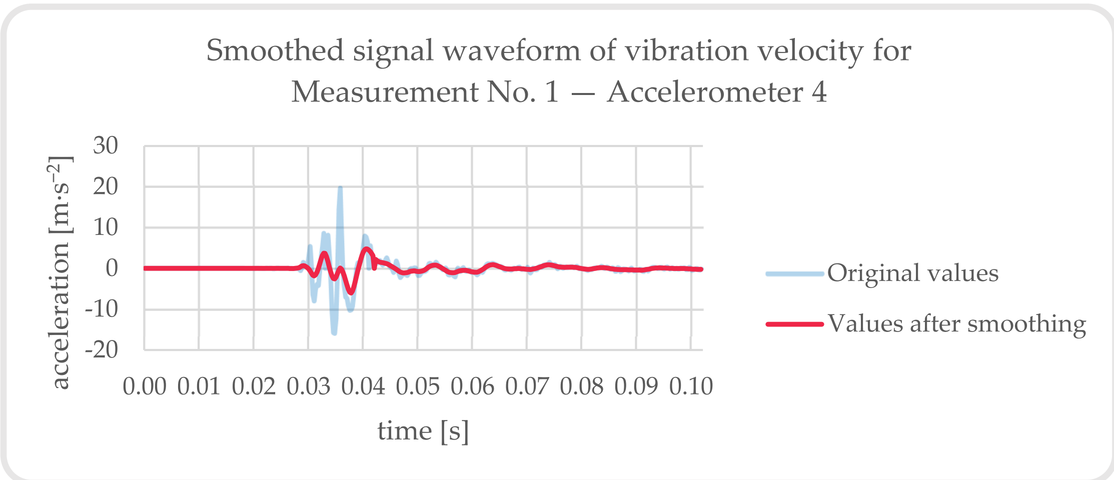

Figure 26. Measurement No. 1—Smoothed vibration velocity time history of Accelerometer 4.

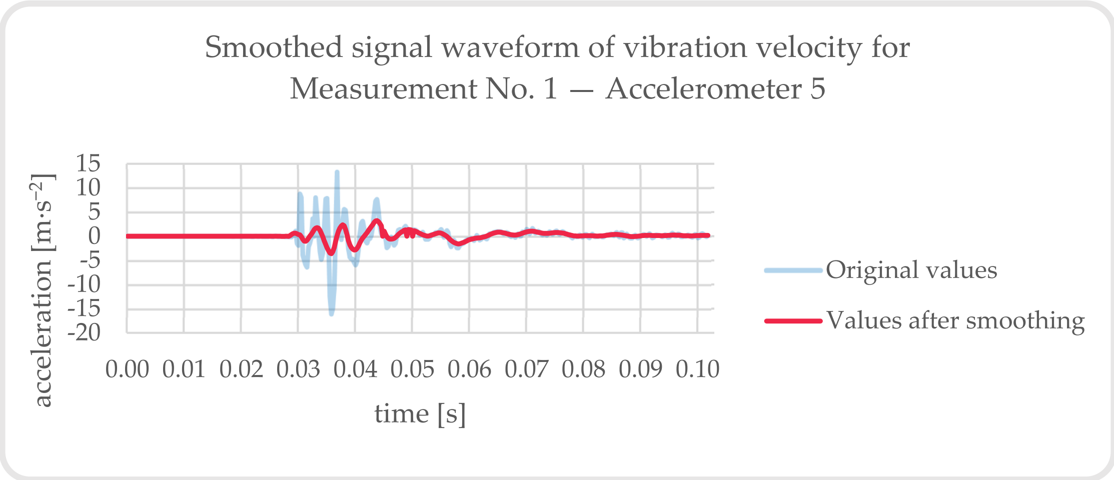

Figure 27. Measurement No. 1—Smoothed vibration velocity time history of Accelerometer 5.

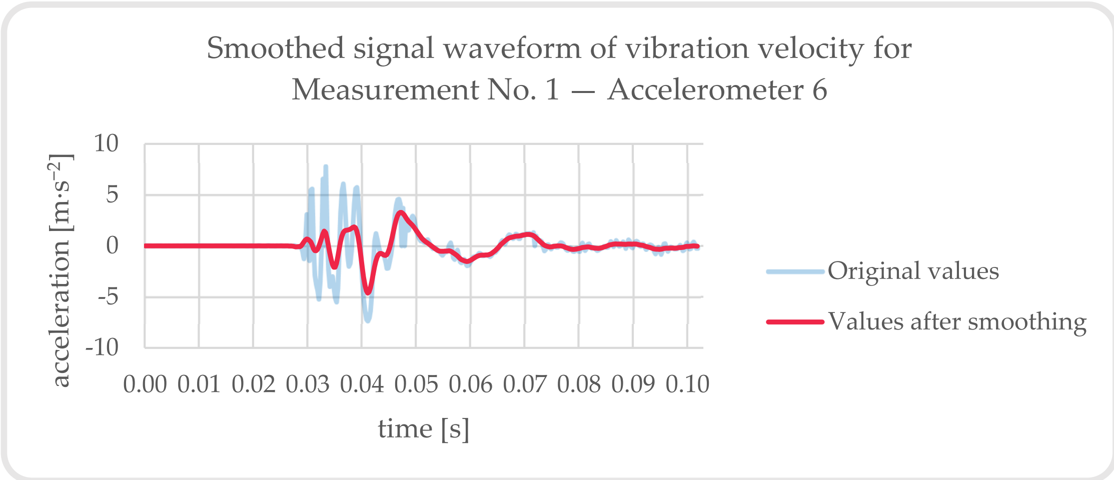

Figure 28. Measurement No. 1—Smoothed vibration velocity time history of Accelerometer 6.

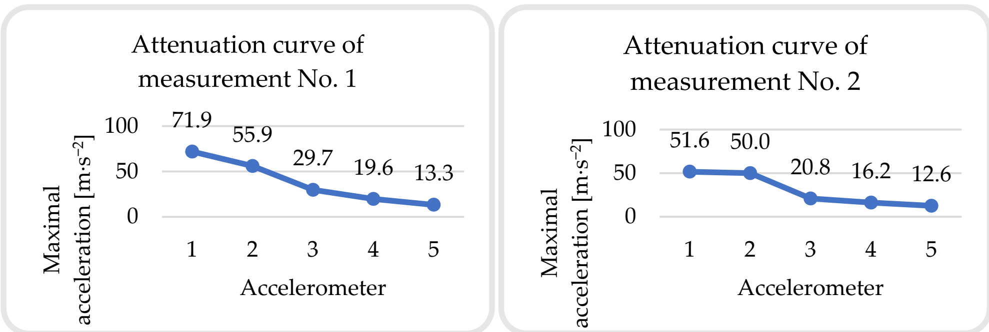

Figure 29. *Cont.*

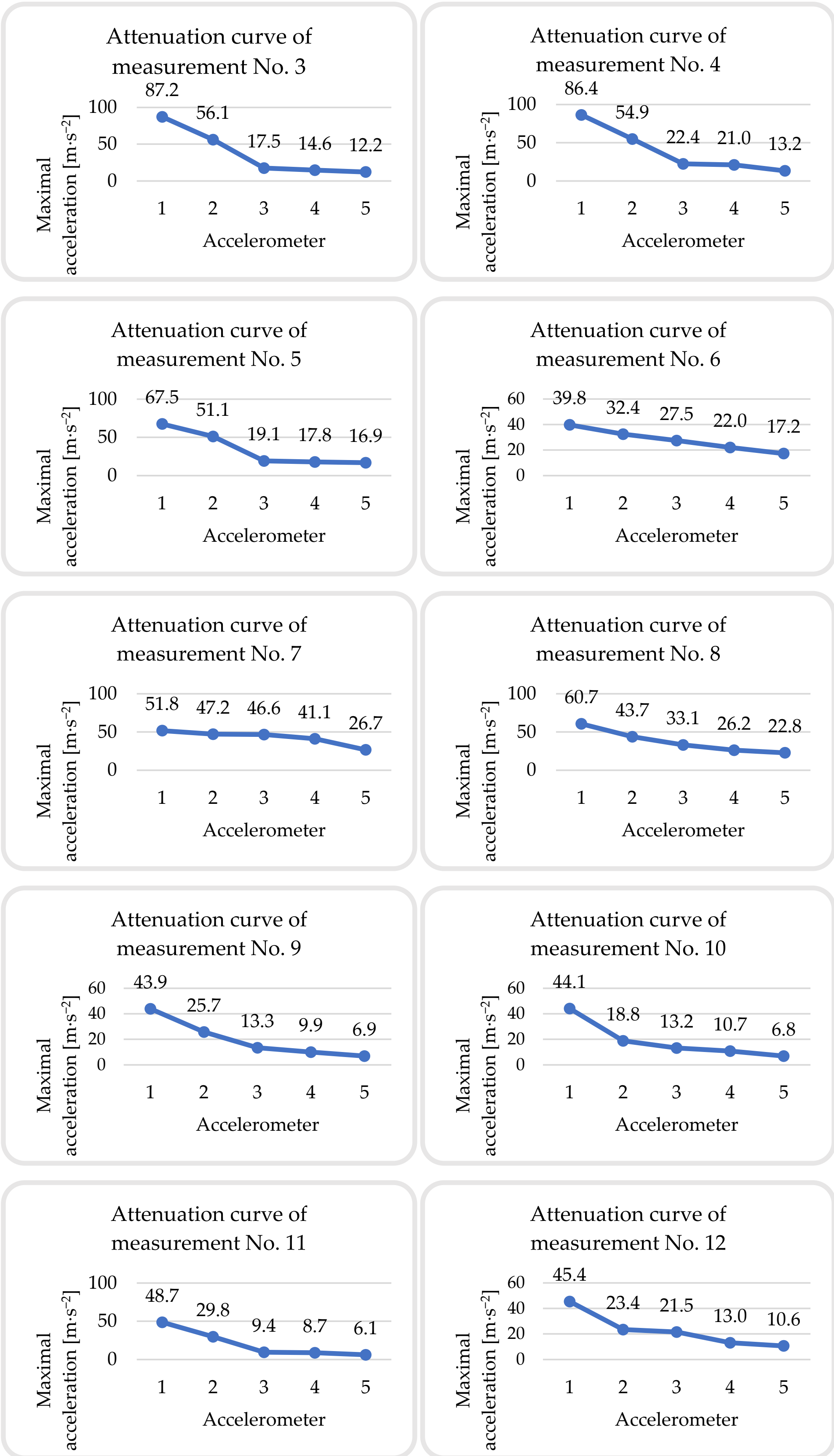

Figure 29. *Cont.*

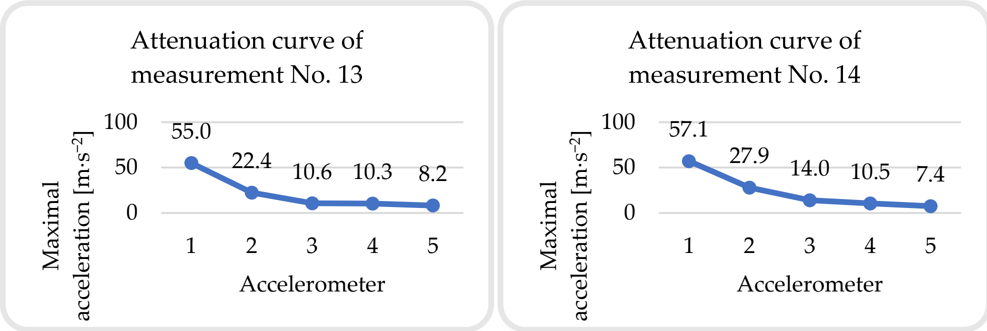

Figure 29. Attenuation curves of all 14 measurements.

A plot of the attenuation curves from all 14 measurements can be seen in Figure 30. It is evident that none of the measurements are identical because they are impacted by a variety of factors. In addition to the particular placement of the firecracker, no two pieces are identical. There is sometimes more active substance, sometimes less, and even the shape does not always match. For this reason, one measurement is insufficient, but multiple measurements must be taken.

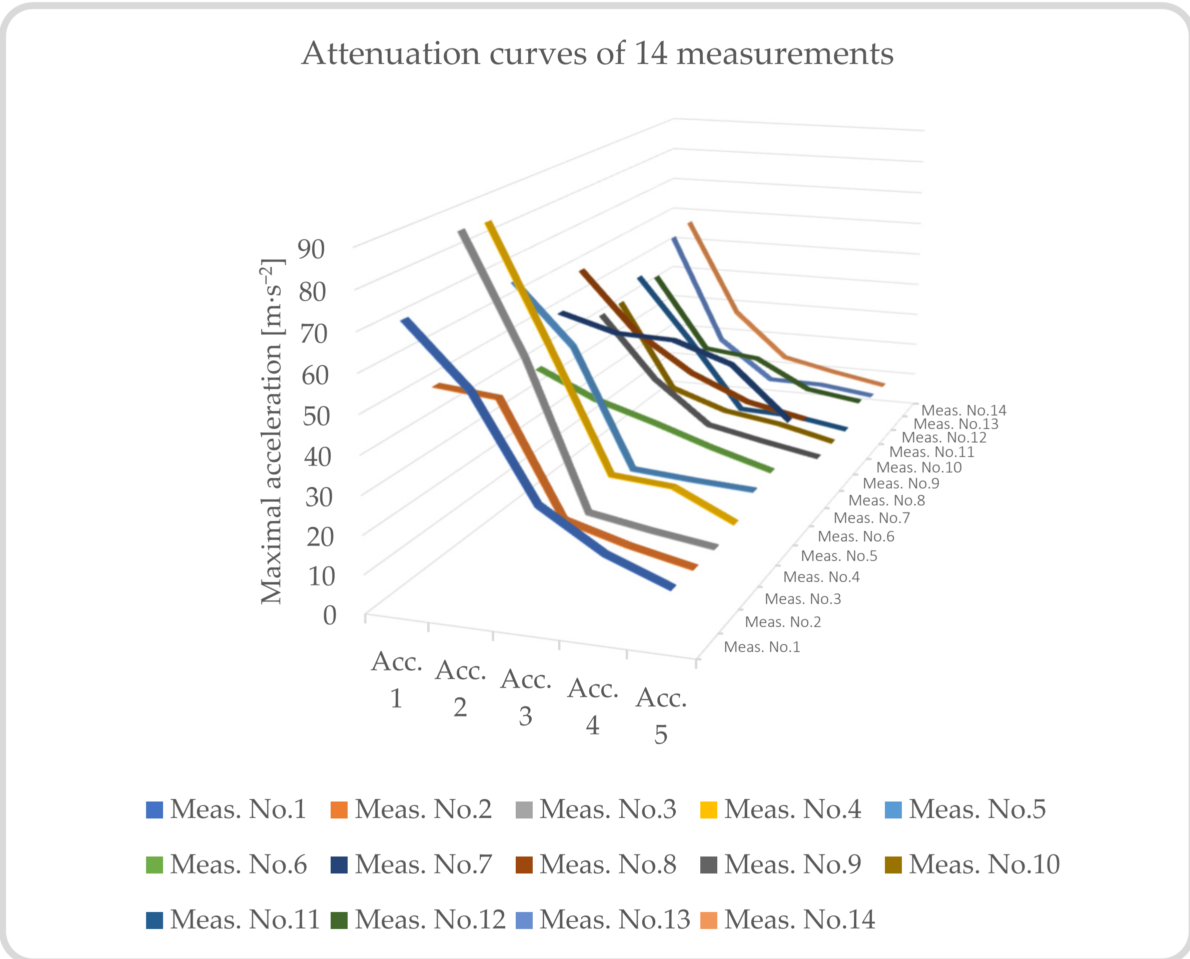

Figure 30. Attenuation curves of all 14 measurements on the small-scale model.

Table 4. Maximum amplitudes of 14 measurements collected on Accelerometers 1–5.

	Maximum Amplitude				
	Accelerometer 1	**Accelerometer 2**	**Accelerometer 3**	**Accelerometer 4**	**Accelerometer 5**
Measurement No.1	71.860	55.928	29.723	19.602	13.276
Measurement No.2	51.600	50.000	20.848	16.176	12.559
Measurement No.3	87.200	56.100	17.456	14.600	12.196
Measurement No.4	86.400	54.900	22.384	21.030	13.216
Measurement No.5	67.500	51.100	19.134	17.848	16.873
Measurement No.6	39.762	32.391	27.452	22.000	17.248
Measurement No.7	51.800	47.200	46.600	41.106	26.651
Measurement No.8	60.700	43.700	33.099	26.171	22.750
Measurement No.9	25.737	43.900	13.322	9.110	6.868
Measurement No.10	44.100	18.827	13.205	10.713	6.845
Measurement No.11	48.700	29.779	9.406	8.743	6.092
Measurement No.12	45.400	23.395	21.538	13.041	10.611
Measurement No.13	55.000	22.376	10.584	10.313	8.211
Measurement No.14	57.100	27.925	14.023	10.470	7.439

4. Discussion

Two main parts of the paper are presented, namely the theoretical section and the experimental section. In the theoretical section, an introduction to explosions and explosives is provided, along with an approach of how energy is calculated in an explosion and types of seismic waves. Experimental measurements were conducted in order to represent the explosion on a small-scale model and demonstrate the occurrence of all types of seismic waves generated during an explosion. Additionally, in this section, the measurement equipment, the simulation material as well as a brief description of the measurement methodology are described. A summary of the measurements is also presented, confirming that dispersive attenuation has occurred, and all types of waves have reached the accelerometers. Additionally, smoothed records, which in this case were not required to be carried out, are shown in the results chapter as an example of how to deal with the records in more detail. Additionally, included is a further detailed figure where each wave type can be seen as it approaches the accelerometers one after the other. As a final conclusion, all measurements are summarized and evaluated in terms of the attenuation curve.

5. Conclusions

The following information will provide a brief overview of the experimental measurement. The presented results confirmed what we already knew about the dispersive attenuation of explosions.

The following graph (Figure 31) represents one of the measurements where dispersive attenuation occurred. Generally, acceleration decreases with increasing distance from the initial explosion point. The measurements confirm that there is a significant difference in acceleration decrement between positions close to and far from an explosion. This is because when an explosion occurs, it creates a shockwave that moves in all directions. The closer you are to the explosion, the more intense this shockwave is.

In the future, more experimental measurements need to be carried out with a larger amount of charge. This will help us better understand how explosives work and how we can better protect structures and their occupants to make them safer.

The research presented in the paper achieves comparable results to research presented in various international publications. Among the first attempts to compare experiment and computation in the field of small-scale models and explosions is the work detailed in [18]. However, similar research applied to RC models is presented in [19]. A detailed analysis of a small-scale explosion site with tracking of fragments and particles scattering can be found in the results of [20]. Another alternative small-scale explosion, the wire explosion, was considered in [21]. Additionally, very comparable results with extensive theoretical-experimental analysis can be found in the scientific study published in [22], where the authors focus on wave processes. At this point, it is still necessary to mention the significant contribution of the publications to the practical tasks of geotechnical engineering focusing on small-scale physical models, which are presented in [23,24]. The implications and applicability of the significance of the presented research work can be found in the practical studies of civil engineering in [25–27]. However, the significance of the presented research is mainly hidden in its potential for further investigation of the presented physical phenomena. This practical research is currently being continued and the correlation of in situ results, numerical calculations, analytical assumptions, and actual full-scale experiment is very interesting and will soon also be presented in a scientific publication. The presented problem has also been addressed by experts in Ljubljana, Slovenia; their results are found in [28–34].

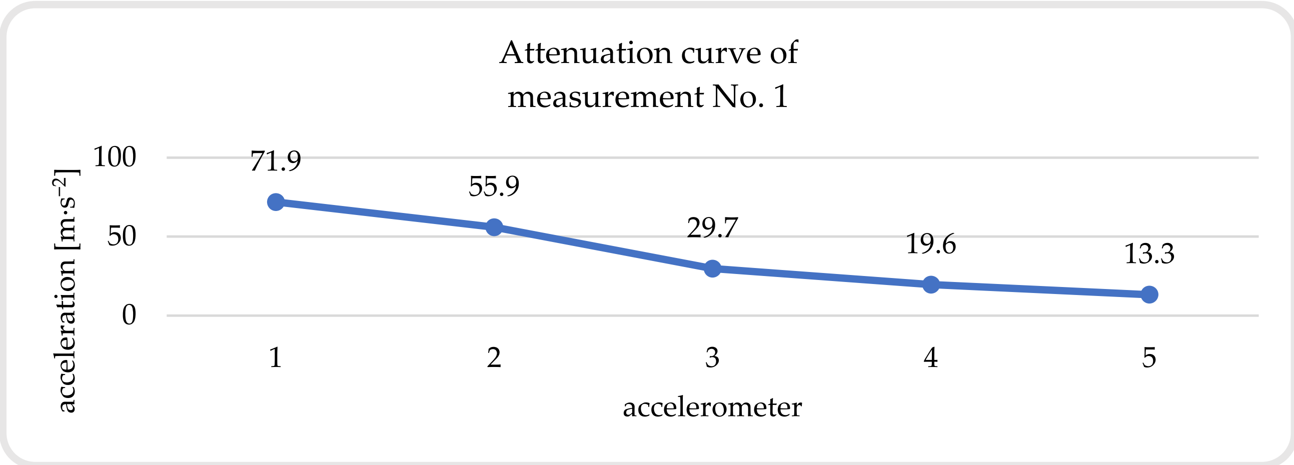

Figure 31. An attenuation curve of measurement No. 1, where the largest value of acceleration is measured by Accelerometer 1, which is closest to the explosion location. The curve gradually decreases until the lowest value is at Accelerometer 5.

Author Contributions: Conceptualization, D.P. and Z.P.; methodology, E.B. and D.P.; software, D.P. and E.B.; validation, Z.P., D.P. and E.B.; formal analysis, Z.P.; investigation, E.B.; resources, E.B. and Z.P.; data curation, Z.P.; writing—original draft preparation, E.B.; writing—review and editing, Z.P. and D.P.; visualization, E.B.; supervision, Z.P.; project administration, D.P.; funding acquisition, D.P. All authors have read and agreed to the published version of the manuscript.

Funding: This research was funded by the Ministry of Education, Science, Research and Sport of the Slovak Republic, grant number VEGA 1/0084/20 "Numerical and experimental analysis of transition areas of objects of structures of railway superstructures and objects of formation substructure".

Informed Consent Statement: Not applicable.

Data Availability Statement: The data presented in this study are available on request from the corresponding author. At the time the project was carried out, there was no obligation to make the data publicly available.

Acknowledgments: This research has been supported by the Project "SPS G5924—Inspection and security by Robots interacting with Infrastructure digital twinS (IRIS)", approved in the framework of the NATO Science for Peace and Security (SPS) Programme.

Conflicts of Interest: The authors declare no conflict of interest. The funders had no role in the design of the study; in the collection, analyses, or interpretation of data; in the writing of the manuscript; or in the decision to publish the results.

References

1. Sakurai, A. *Blast Wave Theory*; Wisconsin Univ-Madison Mathematics Research Center: Madison, WI, USA, 1964; p. 1.
2. Diaz, J.S.; Rigby, S.E. Blast wave kinematics: Theory, experiments, and applications. *Shock Waves* **2022**, *32*, 405–415. [CrossRef]
3. Sapozhnikov, V.B.; Foufoula-Georgiou, E. Experimental evidence of dynamic scaling and indications of self-organized criticality in braided rivers. *Water Resour. Res.* **1997**, *33*, 1983–1991. [CrossRef]
4. Zhao, X. *Fundamental Experimental Studies in Scaling, Blast Mitigation and Material Processing*; University of South Carolina: Columbia, SC, USA, 2013.
5. Taylor, G. The transformation of a blast wave by a very intense explosion. *Proc. R. Soc. A* **1950**, *201*, 159–174.
6. Jack, W.H.; Armendt, B.F., Jr. *Measurements of Normally Reflected Shock Parameters from Explosive Charges under Simulated High Altitude Conditions*; U.S. Army Materiel Command, Ballistics Research Laboratories, Aberdeen Proving Ground: Maryland, MD, USA, 1965; Report No. 1280.
7. Vrba, P. Základy Problematiky Výbuchu a Jejich Vlivl na Stavební Konstrukce. Available online: https://concrete.fsv.cvut.cz/phdworkshop/proceedings/2020/pdf/Vrba_Pavel.pdf (accessed on 1 October 2022).
8. Fay, S. Characterisation of Blast Loading for Shallow Buried Explosives. Ph.D. Thesis, University of Sheffield, Sheffield, UK, 3 September 2020.
9. Janíček, M.; Drahovzal, P. *Pyrotechnik v Boji Proti Terorismu*, 1st ed.; Deus: Praha, Česká Republika, 2001.
10. University of Toronto. Available online: https://www.atmosp.physics.utoronto.ca/people/codoban/PHY138/Mechanics/dimensional.pdf (accessed on 1 October 2022).
11. Atomicarchive.com. Available online: https://www.atomicarchive.com/science/effects/thermal-radiation.html (accessed on 1 October 2022).
12. ScienceNewsExplores. Available online: https://www.snexplores.org/article/explainer-seismic-waves-come-different-flavors (accessed on 1 October 2022).
13. Field, S.Q. *Boom!: The Chemistry and History of Explosives*; Chicago Review Press: Chicago, IL, USA, 2017.
14. Český Úřad pro Zkoušení Zbraní a Střeliva. Available online: https://www.cuzzs.cz/cs/akreditovana-certifikace-pyrotechniky/ (accessed on 1 October 2022).
15. Durham Instruments. Available online: https://disensors.com/product/bk-type-4508-b-002-piezoelectric-ccld-accelerometer-teds-1000-mv-g-1-slot-top-connector-excl-cable/ (accessed on 1 October 2022).
16. SPECMAN. Available online: http://www.specman.pt/assets/lan-xi2.pdf (accessed on 1 October 2022).
17. Metra Mess- und Frequenztechnik in Radebeul, e.K. Available online: https://www.mmf.de/manual/vc21mane.pdf (accessed on 1 October 2022).
18. SIGVIEW. Available online: https://sigview.com/ (accessed on 1 October 2022).
19. STEM MAYHEM. Available online: https://www.stemmayhem.com/how-does-kinetic-sand-work/ (accessed on 1 October 2022).
20. Courtney, C.E. *Mechanical Behavior of Materials*, 2nd ed.; Waveland Press, Inc.: Long Grove, IL, USA, 2005.
21. IOPscience. Available online: https://iopscience.iop.org/article/10.1088/0960-1317/24/3/035017/pdf (accessed on 1 October 2022).
22. Zyskowski, A.; Sochet, I.; Mavrot, G.; Bailly, P.; Renard, J. Study of the explosion process in a small scale experiment—Structural loading. *J. Loss Prev. Process Ind.* **2004**, *17*, 291–299. [CrossRef]
23. Zhao, C.; Wang, Q.; Lu, X.; Huang, X.; Mo, Y.L. Blast resistance of small-scale RCS in experimental test and numerical analysis. *Eng. Struct.* **2019**, *199*, 109610. [CrossRef]
24. Hassan, Z.A.; Ibrahim, A.; Nor, N.M. Feasibility of a small-scale test apparatus in measuring blast intensity of shallow buried charge detonation in in-situ soil. *Sci. Technol. Energetic Mater.* **2019**, *80*, 229–236.
25. Sadot, O.; Ram, O.; Nof, E.; Kochavi, E.; Ben-Dor, G. Small-scale blast wave experiments by means of an exploding wire. In *Blast Effects*; Springer: Cham, Germany, 2018; pp. 141–170.
26. Scalise, M.; Pitarka, A.; Louie, J.N.; Smith, K.D. Effect of random 3D correlated velocity perturbations on numerical modeling of ground motion from the Source Physics Experiment. *Bull. Seismol. Soc. Am.* **2021**, *111*, 139–156. [CrossRef]
27. Zhuang, X.; Zong, Z.; Huang, Y.; Wang, P. Analysis of the Installation Effect on the Axial Performance of Pressure-Grouted Helical Piles in Clay by Small-Scale Model Tests. *Buildings* **2022**, *12*, 992. [CrossRef]
28. Nujaim, M.; Belem, T.; Giraud, A. Experimental Tests on a Small-Scale Model of a Mine Stope to Study the Behavior of Waste Rock Barricades during Backfilling. *Minerals* **2020**, *10*, 941. [CrossRef]
29. Caçoilo, A.; Mourão, R.; Belkassem, B.; Teixeira-Dias, F.; Vantomme, J.; Lecompte, D. Blast wave assessment in a compound survival container: Small-scale testing. *Multidiscip. Digit. Publ. Inst. Proc.* **2018**, *2*, 540.
30. Papán, D.; Valašková, V.; Drusa, M. Numerical and experimental case study of blasting works effect. In *IOP Conference Series: Earth and Environmental Science*; IOP Publishing: Bristol, UK, 2016; Volume 44, p. 052052.
31. Ainalis, D.; Kaufmann, O.; Tshibangu, J.P.; Verlinden, O.; Kouroussis, G. Modelling the source of blasting for the numerical simulation of blast-induced ground vibrations: A review. *Rock Mech. Rock Eng.* **2017**, *50*, 171–193. [CrossRef]
32. Trajkovski, J.; Kunc, R.; Perenda, J.; Prebil, I. Minimum mesh design criteria for blast wave development and structural response-MMALE method. *Lat. Am. J. Solids Struct.* **2014**, *11*, 1999–2017. [CrossRef]

33. Trajkovski, J.; Perenda, J.; Kunc, R. Blast response of Light Armoured Vehicles (LAVs) with flat and V-hull floor. *Thin-Walled Struct.* **2018**, *131*, 238–244. [CrossRef]
34. Trajkovski, J.; Kunc, R.; Prebil, I. Blast response of centrally and eccentrically loaded flat-, U-, and V-shaped armored plates: Comparative study. *Shock Waves* **2017**, *27*, 583–591. [CrossRef]